DIRECT LYAPUNOV EXPONENT ANALYSIS ENABLES PARAMETRIC STUDY OF TRANSIENT SIGNALING GOVERNING CELL BEHAVIOR

Bree B. Aldridge[1,2], George Haller[3], Peter K. Sorger[1,2], and Douglas A. Lauffenburger[1,2,*]

[1]Biological Engineering Division, [2]Center for Cell Decision Processes, [3]Department of Mechanical Engineering, MIT, Cambridge MA 02139

Running Title: Parametric Study of Transient Signaling

Keywords: differential equation models, apoptosis, caspase, Lyapunov exponent, systems analysis, applied nonlinear dynamics, sensitivity analysis, steady-state analysis, transient signal, signal transduction, stability analysis

*Corresponding author address
Douglas A. Lauffenburger
Biological Engineering Division
56-341
MIT
Cambridge, MA 02139
617-252-1629 (telephone)
617-258-0204 (fax)
lauffen@mit.edu (email)

Additional author addresses
Bree B. Aldridge
Biological Engineering Division
68-371, MIT
Cambridge, MA 02139
breea@mit.edu (email)

George Haller
Department of Mechanical Engineering
3-352, MIT
Cambridge, MA 02139
ghaller@mit.edu (email)

Peter K Sorger
Biological Engineering Division
68-371, MIT
Cambridge, MA 02139
psorger@mit.edu (email)

ABSTRACT

Computational models aid in quantitative understanding of cell signaling networks. One important goal is to ascertain how multiple network components work together to govern cellular responses – *i.e.*, to determine cell "signal-response" relationships. Several methods exist to study steady-state signals in the context of differential equation-based models. However, many biological networks influence cell behavior through time-varying signals operating during a transient activated state which ultimately returns to a basal steady-state. We describe a computational approach adapted from dynamical systems analysis to discern how diverse transient signals relate to alternative cell fates. We employ direct finite-time Lyapunov exponents (DLEs) to identify phase-space domains of high sensitivity to initial conditions. These domains delineate regions exhibiting qualitatively different transient activities that would be indistinguishable using steady-state analysis but which correspond to different outcomes. We apply these methods to a physico-chemical model of molecular interactions among caspase-3, caspase-8, and XIAP – proteins whose transient activation determines cell death-vs-survival fates. DLE analysis enabled identification of a separatrix that quantitatively characterizes network behavior by defining initial conditions leading to apoptotic cell death. We anticipate that DLE analysis will facilitate theoretical investigation of phenotypic outcomes in larger models of signaling networks.

.

1 INTRODUCTION

Reaction models employing differential equations are frequently used as tools for computational exploration of complex biomolecular networks, such as those involved in signal transduction of extracellular stimuli governing cell fate. These models, generally based on mass-action kinetics, incorporate network topology and quantitatively describe the kinetics of interactions between network components [1-8]. Because these mechanistic models are large and complicated, quantitative analysis is necessary to extract understanding [6, 9]. A typical objective of model analysis is to comprehensively characterize the response of the signaling network to changes in system parameters. By altering network behavior, changes to protein levels or reaction rates may lead to different cell fates following exogenous stimulation [10-13]. As an example, activation of the small GTP-binding protein Ras can induce a variety of cell responses including cell proliferation and differentiation, depending on the cell type and extracellular conditions. Perturbations to the Ras-mediated regulatory network can promote pathological cell behavior; mutations that affect Ras levels or binding or reaction rates are often linked to cancer [14]. Numerous similar examples may be found underlying cell behavioral dysregulation; thus, illuminating how changes in molecular interactions alter signaling network behavior is key to understanding the molecular basis of disease. Simulations can be used to inspect signaling behavior arising from network perturbations of potential interest – perhaps a genetic mutation or pharmacological intervention [6, 15]. By simulating a mechanistic model, predictions can be made about how specific changes to parameters such as stimulation or drug inhibition conditions, initial concentrations, and reaction rates will affect signaling [4, 16-21]. To link different cell responses to complex signaling interactions, however, more systematic, comprehensive analysis methods need to be applied.

Common systematic tools for studying the behavior of differential equation models for signaling networks include parameter sensitivity analysis and steady-state analysis. Determining sensitivity to rate constants and initial conditions (*i.e.*, protein levels at the initial time point) is useful for finding reactions and species that are particularly important in the overall reaction scheme [22-24]. However, the local sensitivities that may arise from intertwined multivariate interactions cannot be revealed by single-parameter sensitivity analysis. A comprehensive analysis, where several parameters are changed simultaneously, is often computationally impractical and the results intractable. The analysis method presented in this work is based on direct Lyapunov exponents (DLEs), which is a comprehensive local sensitivity analysis of model initial conditions. The DLE approach can be interpreted in a manner that is analogous to steady-state analysis of metabolic networks. Our analysis goal is to understand how the qualitative network behavior (essentially, the biological fate) depends on the quantitative combinations of network component parameters (essentially, the network state).

Steady-state analysis methods have been established in dynamical systems as powerful methods for analyzing models of a variety of physico-chemical processes, including fluid flow and chemical reactions. These techniques, including fixed-point bifurcation methods, have been successfully used to study several biological network models. These methods delineate how changes in initial conditions and rate parameters affect the biological outcomes associated with different equilibria. Good candidates for this analysis are systems with multiple steady steady-states, where each phenotypic behavior is associated with a particular steady-state. Examples include metabolic networks, the cell cycle, and engineered gene networks [2, 5, 25-27]. In contrast, many signal transduction networks affect cell fate through transient, pre-steady-state signals. Here, we will refer to these systems as “transient response networks”. In transient

response networks, rapidly-changing signals, or transients, induce changes in other signals that propagate through the pathways [10, 19, 20, 28]. In these systems, the time-evolution of transient signals, not steady-state signals, influences cell behavior. For this reason, transient response systems may not be good candidates for steady-state analysis. To understand these systems, we require methods that analyze transient signals, such as DLE analysis described here.

The transient response system that we analyze in this work is a core sub-network of the signal transduction cascade regulating the programmed cell death (apoptosis)-versus-survival phenotypic decision. Apoptosis has in some previous work been modeled as a bistable system where death and survival are distinct stable steady-states [29, 30]. However, this is not the only way, nor necessarily the most appropriate way, to cast a problem that appears to involve a transient response network [28, 31]. In fact, models focusing on the later stages of the apoptotic decision such as ours as well as one of the alternative models developed by Eissing et al. do not exhibit bistablity [29]. In response to apoptotic stimuli, this network produces a transient response that is dependent on the stimuli and the state of the cell. The transient signals will either lead to apoptosis (where the network does not reset because the cell dies) or survival (where the network resets).

Apoptosis is induced by extrinsic (receptor-dependent) and intrinsic (intracellular) pathways. Common to both pathways is the activation of caspases, a family of proteases that execute the cell death decision by cleaving protein targets. The caspases activate each other to form a protease cascade and are themselves subject to regulation by many other proteins [32-34]. Caspases are synthesized in an inactive state (pro-caspases or zymogens) and become active when dimerized or cleaved by other caspases. Intracellular or extracellular pro-death stimuli lead to dimerization and cleavage of initiator caspases such as caspase-8. Once activated, these

initiator caspases in turn cleave and activate effector caspases such as caspase-3 (Figure 1). Activation of initiator by effector caspases generates positive feedback that can amplify this cascade [32, 35]. Prolonged activation of effector caspases leads to programmed cell death. A critical inhibitor is X-linked inhibitor of apoptosis (XIAP), which negatively regulates the enzymatic activity of caspase-3. Additionally, XIAP tags active caspase-3 for ubiquitination. This modification promotes caspase-3 degradation and causes caspase-3 activity to be transient [36, 37].

Analogous to the application of steady-state analyses to signaling networks where equilibria correspond to cell response, we describe direct finite-time Lyapunov exponent (DLE) analysis as a method to study transient response signaling networks. We use DLEs to analyze how transient signaling dynamics are affected as different parameters change individually or simultaneously in multidimensional phase-space (the set of initial chemical species concentrations). DLE analysis is not the first method to measure local sensitivity analysis, but is distinguished from previously applied techniques because DLEs are calculated as parameters change simultaneously, not individually [23]. DLEs were originally used to find invariant manifolds in dynamical systems and fluid flows [38-41]. Similarly, we use DLEs to find separatrices, or sensitive regions in phase-space that separate signals giving rise to different responses. Separatrices are useful because they quantitatively identify points at which continuous change in species concentration lead to dramatic, discontinuous change in response. As an example of current interest in molecular cell biology, we used DLEs to analyze a small, mechanistic model of a transient response network describing caspase-3 activation in the network described above. We were able to characterize initial conditions (concentrations of protein species) leading to survival and apoptosis with the DLE-defined separatrix, but not by

examining steady-states. We thereby gained conceptual insight into the integrated effects of multiple components in this network.

2 METHODS

2.1 Caspase-3 activation model

A system of ordinary differential equations describing the activation of caspase-3 by caspase-8 was constructed using mass-action kinetics and the known topology of this portion of the apoptosis regulatory network (Figure 1). We have made the following central assumptions: [a] chemical species are present at spatially-uniform concentrations; [b] caspase-6 is not involved in the feedback between active caspase-3 and caspase-8; [c] ubiquitination can be represented by a single lumped reaction; and [d] caspase activation is achieved after an inactive caspase interacts with an active caspase. The differential equation describing the concentration of active caspase-3 tagged for ubiquitination (x_9) was removed from the model because it does affect network. Values for the rate constants are listed in Table 1. The equations defining the model are as follows:

$$\dot{x}_1 = -k_1 x_4 x_1 + k_{d1} x_5 \quad (1)$$

$$\dot{x}_2 = k_{d2} x_5 - k_3 x_2 x_3 + k_{d3} x_6 + k_{d4} x_6 \quad (2)$$

$$\dot{x}_3 = -k_3 x_2 x_3 + k_{d3} x_6 \quad (3)$$

$$\dot{x}_4 = k_{d4} x_6 - k_1 x_4 x_1 + k_{d1} x_5 - k_5 x_7 x_4 + k_{d5} x_8 + k_{d2} x_5 \quad (4)$$

$$\dot{x}_5 = -k_{d2} x_5 + k_1 x_4 x_1 - k_{d1} x_5 \quad (5)$$

$$\dot{x}_6 = -k_{d4} x_6 + k_3 x_2 x_3 - k_{d3} x_6 \quad (6)$$

$$\dot{x}_7 = -k_5 x_7 x_4 + k_{d5} x_8 + k_{d6} x_8 \quad (7)$$

$$\dot{x}_8 = k_5 x_7 x_4 - k_{d5} x_8 - k_{d6} x_8 \quad (8)$$

2.2 Direct finite-time Lyapunov exponent (DLE)

The DLE is a measure of local sensitivity to changes in initial conditions, evaluated multidimensionally at a finite-time, as depicted for one dimension in Figure 2. First, for a selected trajectory, the derivative of the current trajectory position with respect to its initial location is calculated in all independent directions at each finite time instant of interest. These

directional derivatives are in turn assembled into a time-dependent gradient matrix, whose entries are indicative of the rate at which neighboring trajectories separate in the corresponding directions. The spectral norm (or largest singular value) of the gradient matrix gives the instantaneous maximal rate of local trajectory separation over all directions. The DLE associated with the selected trajectory is then defined as the time-averaged logarithm of the above norm, measuring the maximal rate of exponential separation between the underlying trajectory and nearby trajectories. By definition, large DLE values reveal large local sensitivity in the flow with respect to changes in initial conditions.

In numerical computations, we select a sufficiently dense grid of initial conditions for which numerical differentiation gives meaningful results. We then launch trajectories from each grid point and calculate the DLE value defined above for each trajectory. We plot the resulting DLEs over the initial grid to identify locations of highly sensitive initial conditions. Regions of phase-space exhibiting different qualitative behaviors are necessarily separated by sensitive initial conditions, and hence their boundaries (separatrices) will appear as local maximizers of the DLE field. The accuracy of separatrix locations obtained in this fashion will increase as the initial grid size is refined. By the continuous dependence of trajectories on initial conditions, separatrices are captured by our procedure even if they do not exactly intersect the initial grid. This is because separatrices have whole neighborhoods of increased sensitivity, which are captured by a dense enough initial grid.

DLEs, apart from their application described here, are particularly useful in finding repelling and attracting surfaces and have been used in fluid mechanics [40, 41] and rigid body dynamics [41]. In [38, 39], we proved that DLEs robustly identify the locations of maximum stretching (divergence between nearby trajectories). We use the maximum stretching among all

dimensions to measure the rate of exponential separation for a finite-time between two neighboring trajectories (Figure 2).

To quantify the degree of stretching at particular initial conditions, first we define the separation (9) and approximate it by linearization (10).

$$\boldsymbol{\zeta}(t) = \mathbf{x}(t, t_0, \mathbf{x}_0 + \boldsymbol{\zeta}_0) - \mathbf{x}(t, t_0, \mathbf{x}_0) = \frac{\partial \mathbf{x}(t, t_0, \mathbf{x}_0)}{\partial \mathbf{x}_0}\boldsymbol{\zeta}_0 + \mathrm{O}(\left|\boldsymbol{\zeta}_0\right|^2) \qquad (9)$$

$$\boldsymbol{\zeta}(t) \cong \frac{\partial \mathbf{x}(t)}{\partial \mathbf{x}_0}\boldsymbol{\zeta}_0 \qquad (10)$$

Here $\mathbf{x}$ and $\boldsymbol{\zeta}$ are vectors describing species concentration and trajectory separation, respectively. Next, we define stretching as the matrix (spectral) norm of the deformation gradient $\frac{\partial \mathbf{x}(t)}{\partial \mathbf{x}_0}$. Recalling

$$\left\|\mathbf{A}\right\| = \left(\lambda_{\max}\left(\mathbf{A}^T\mathbf{A}\right)\right)^{1/2} \qquad (11)$$

for a square matrix $\mathbf{A}$ (where $\lambda_{\max}(\mathbf{X})$ denotes the maximum eigenvalue of $\mathbf{X}$), we obtain

$$\left\|\frac{\partial \mathbf{x}(t)}{\partial \mathbf{x}_0}\right\|^2 = \lambda_{\max}\left(\left(\frac{\partial \mathbf{x}(t)}{\partial \mathbf{x}_0}\right)^T\left(\frac{\partial \mathbf{x}(t)}{\partial \mathbf{x}_0}\right)\right). \qquad (12)$$

We then define the finite-time maximal (over all directions) stretching rate experienced along the trajectory $\mathbf{x}(t, t_0, \mathbf{x}_0)$ as

$$\frac{1}{t - t_0}\log\left\|\frac{\partial \mathbf{x}(t)}{\partial \mathbf{x}_0}\right\| = \frac{1}{2(t - t_0)}\log\left[\lambda_{\max}\left(\left(\frac{\partial \mathbf{x}(t)}{\partial \mathbf{x}_0}\right)^T\left(\frac{\partial \mathbf{x}(t)}{\partial \mathbf{x}_0}\right)\right)\right]. \qquad (13)$$

Note that we can treat $\frac{1}{2(t - t_0)}$ as a constant because the stretching rates are compared at a particular time *t*. Therefore, we can further simplify (13) to define the DLE by factoring out this constant:

$$DLE(t,\mathbf{x}_0)=\log\left[\lambda_{\max}\left(\left(\frac{\partial\mathbf{x}(t)}{\partial\mathbf{x}_0}\right)^T\left(\frac{\partial\mathbf{x}(t)}{\partial\mathbf{x}_0}\right)\right)\right]. \quad (14)$$

2.3 DLE computation and visualization

Classical finite-time Lyapunov exponents are typically computed for

$$\dot{\mathbf{x}}=\mathbf{f}(\mathbf{x},t) \quad (15)$$

by numerically solving the linear system

$$\dot{\boldsymbol{\zeta}}=\frac{\partial\mathbf{f}}{\partial\mathbf{x}}(\mathbf{x}(t,t_0,\mathbf{x}_0),t)\boldsymbol{\zeta}, \quad (16)$$

obtained from differentiating (10) in time. By contrast, DLEs are computed directly from (10), without the laborious solution of (16) along all trajectories. Specifically, we compute finite-time Lyapunov exponents directly by differentiating final trajectory positions with respect to their initial condition (hence the terminology "direct" Lyapunov exponent).

To compute DLEs, a grid of initial conditions sampling phase-space was chosen, and each set of initial conditions was integrated with respect to time using the ode15s solver in MATLAB 7.0 (The Mathworks, Natick, Massachusetts). The deformation gradient $\frac{\partial\mathbf{x}(t)}{\partial\mathbf{x}_0}$ was then obtained from a numerical differentiation of final trajectory position with respect to their initial conditions. Next, the natural log of the maximum eigenvalue of the strain tensor $\left(\frac{\partial\mathbf{x}(t)}{\partial\mathbf{x}_0}\right)^T\left(\frac{\partial\mathbf{x}(t)}{\partial\mathbf{x}_0}\right)$ was computed to find the DLE, as defined in (14), at each initial condition.

For a grid of approximately $1.6\text{x}10^6$ points, the entire computation (including trajectory integration) was completed in approximately 85 hours on a Linux workstation with 2 GB of memory and dual 2.80 GHz Intel Xeon processors. The points on the grid were linearly spaced

along each direction. The MATLAB code performing the computation is provided at http://cdp.mit.edu/. The resulting DLEs were visualized using Spotfire DecisionSite (Spotfire, Somerville, Massachusetts).

3 RESULTS

3.1 The cell phenotypic response of apoptotic death is governed by transient signals in a caspase-mediated network

As a test case of a biologically-important transient response network, we explored a mechanistic, differential equation-based model of caspase-3 activation depicted in Figure 1. This network includes both pro-apoptotic elements (caspase-8 and caspase-3) and a pro-survival factor (XIAP). While it has only eight distinct species (and dimensions), our caspase-3 activation model is complex enough to be obscure without analysis.

In the presence of active caspase-8, this network produces a transient response that is dependent on the initial conditions (concentrations) of the eight network species (Figures 3A-B). In cells, apoptosis is triggered by elevated and prolonged caspase-3 (or effector caspase) activation. Figure 3 shows simulated time courses (trajectories) from our model, where apoptotic cells are categorized as exhibiting a relatively tall and wide pulse of active caspase-3, while surviving cells are characterized by short and narrow spikes of active caspase-3. As expected in a transient response system, we observe that after loss of the transient signal, pro- and anti-apoptotic time courses eventually reach the same type of steady-state (Figures 3C-3D). A careful look at the time-scale shows that it takes nearly a week for the pro-death signal to reach equilibrium. In reality, such a cell would have died before the end of two days, and this steady-state would never be reached. For simplification, this model does not include protein turnover. We observed that the introduction of turnover into our model did not significantly change its response (Supplementary Materials).

This preliminary inspection of the caspase-3 activation model demonstrates that transient signals for pro- and anti-apoptotic conditions differ qualitatively. These two types of trajectories separate from one another before reaching steady-state. Furthermore, the behavior of the network is dependent on initial conditions. By increasing the initial concentration of XIAP, the transient signal changes from a pro-apoptotic to a pro-survival signal (Figure 3). We anticipate that there is a sensitive initial condition of XIAP at which the behavior of the network changes, and that this sensitive point will shift according to initial conditions of the active and inactive caspases.

3.2 Large DLEs define a separatrix separating phase-space into pro- and anti-apoptotic regions

As described in the Introduction and Methods sections, we employ direct Lyapunov exponents (DLEs) to search our model phase-space for regions delineating diverse behavior of transient network signals related to different cell phenotypic responses (see Figure 2). Neighboring trajectories in these regions will veer away from each other, thus exhibiting large DLEs that effectively define separatrices dividing the phase-space into regions possessing different trajectory behaviors. Because DLEs are calculated for the endpoint of the trajectories, they depend on the specific time-point at which the trajectory separation is measured. This feature is a crucial aid in studying transient response systems, for it insures that the analysis can be performed based on transient signals.

To characterize the network's dependence on initial conditions in multiple dimensions, we computed DLEs across an eight-dimensional grid spanning a wide range of initial species concentrations. Totaling approximately 1.6×10^6 points, the grid points are linearly spaced

along each direction. These concentrations were chosen to encompass protein expression across cell populations and under different signaling conditions in Hct-116, HeLa, and HT-29 carcinoma cell lines (10^2-10^5 molecules/cell for XIAP and 10^2-$3.5x10^6$ molecules/cell for the caspases [S. Gaudet and K. Leitermann, personal communication]). Biochemical intermediates were sampled with coarser resolution because they were not found to contribute to the network behavior (data not shown). To find a separatrix, DLEs were calculated at six hours, by which time Hct-116, HT-29, and HeLa cells would have responded to treatment with death-inducing ligands Tumor Necrosis Factor (TNF) or TNF-related apoptosis-inducing ligand (TRAIL) [B. Aldridge, unpublished observations]. To determine how narrow the time-window of effective separatrix appearance might be, we additionally undertook DLE calculations across the range between two and twelve hours, and found that the separatrix did not move noticeably (data not shown).

Since it is problematic to simultaneously visualize the phase-space in eight-dimensions, in Figure 4 we offer more accessible illustrations of the DLEs in three-dimensional slices. Figure 4A illustrates the DLEs in the subspace containing XIAP, caspase-8, and active caspase-8, whereas Figure 4B shows the DLEs in the subspace containing XIAP, active caspase-8, and active caspase-3. Large DLEs (blue) define a finite-time separatrix that identifies the points at which the balance between XIAP and active caspase-8 shifts so that the overall response changes from pro-apoptotic to anti-apoptotic signals. We expected the apoptosis regulatory network to have a separatrix because the cell's response is either survival or death – it is not graded (from alive to sick to dead). If a system were to exhibit a more graded response, the DLEs would have been more uniform across phase-space and would not have yielded a discernible separatrix.

The location and shape of the separatrix provide a framework to generate conceptual interpretation of network operation. The separatrix shifts towards higher XIAP concentrations as the amount of active caspase-8 increases (Figure 4A). Cells will die if above the separatrix, whereas below the separatrix there is enough XIAP to overcome the conversion of inactive caspase-3 to active caspase-3 by active caspase-8. The separatrix shape is invariant to inactive caspase-8, suggesting that the positive feedback activating caspase-8 by caspase-3 has less influence than the regulation of caspase-3 by active caspase-8 and XIAP. Since XIAP tags active caspase-3 for degradation, more XIAP would be needed to rescue the cell from a death decision if there was a higher initial concentration of active caspase-3 (Figure 4B). Figure 4C shows perturbations to the separatrix as the ubiquitination rate constant is changed. As the rate increases, so does the slope of the separatrix in the XIAP and active caspase-8 subspace. The slower the ubiquitination rate, the longer the complex of active caspase-3 and XIAP will exist, effectively lowering the concentration of free XIAP. We also observed that the separatrix is not a simple plane – it curves at higher concentrations of active caspase-8 and shifts slope as the ubiquitination rate changes (Figure 4C).

In addition to using the separatrix as a tool to help us interpret the decision-making mechanisms of the network, the separatrix quantitatively identifies the critical ratios of initial conditions around which the cell response changes. By comparing the location of different cells in phase-space to each other and the separatrix, we can evaluate how differences in species concentrations affect differential cell behavior. It is informative to note that the location of a cell in phase- or concentration-space affects how the network reacts to signals. For example, consider two cells in the pro-apoptotic section of phase-space that have different XIAP concentrations (as indicated in Figure 4B). The purple and red starred cells are close to and far

from the separatrix, respectively. The red starred cell requires an eight-fold increase in XIAP concentration to cross the separatrix (to reach the green star) while the purple starred cell needs a modest two-fold increase. Alternatively, the red starred cell could move to the separatrix by increasing its XIAP concentration six-fold while decreasing its active caspase-8 concentration by one half (orange star). If the XIAP concentration is increased four-fold in both cells, the cells will behave differently and only the purple starred cell will cross the separatrix to survive. This simple example illustrates that we need to know the cell's state (key species concentrations) before predicting response. The DLE-defined separatrix helps us understand how cells in different states can have disparate responses to the same stimulation or perturbation.

3.3 A steady-state analysis cannot distinguish pro- and anti-apoptotic responses across phase-space

Direct analysis of the set of nonlinear algebraic equations representing our model at steady-state showed that the system has four types of equilibria (*i.e.*, four invariant manifolds filled with fixed points, in contrast to four fixed points) with only one type being stable (Figure 5A, Supplementary Materials). These stable fixed points can have non-zero valued concentrations of caspase-8 and XIAP. However, the concentration of caspase-3 must be zero because any inactive caspase-3 would be activated by caspase-8 and subsequently degraded by XIAP before a steady-state is reached. The phase-space locations of these stable fixed points are dependent on initial conditions.

To investigate whether these stable steady-states segregate into pro- and anti-apoptotic clusters, we plotted the steady-state locations from small subsets of trajectories. Figures 5B-D show active and inactive caspase-8 equilibrium concentrations from different small sets of

trajectories. Within each set, the initial conditions of inactive caspase-8 were constant and most steady-states cluster into death or survival locales. For example, cells that survive stimulation with a death stimulus generally have low active and high inactive caspase-8 concentrations because caspase-3 was not activated enough to convert most of the inactive caspase-8 to the active form. This suggests that within a small set of initial conditions, a separatrix can be identified by plotting stable fixed points.

However, when we plotted trajectories from a broader range of initial concentrations of caspase-8, the ability to distinguish cell fate based on steady-state locations is lost (Figure 5E). In contrast, DLEs can separate the two fates without considering steady-state values. We have seen in Figure 4 that large DLEs can define a separatrix over a broad set of initial conditions. For the small sets described above, equilibria between the clusters have large DLEs and separate the groups representing surviving and dying cells (Figure 5B-D). We conclude that DLEs are versatile and can be applied regardless of whether or not steady-states cluster by behavior (Figure 5F).

4 DISCUSSION

Our goal here is to develop an analysis methodology for differential equation models aimed at understanding how transient signals influence phenotypic responses – *i.e.*, to develop signal-response relationships for most transient response networks in higher cells. Many signal transduction networks are transient response networks, meaning that they affect phenotypic cell responses before a steady-state is reached. Therefore, the steady-state and bifurcation analysis methods traditionally used to study differential equation-based models do not find straightforward application to transient response networks. To successfully analyze complex networks, we required that our methodology be applicable to transient signals across multiple dimensions.

Towards this challenging goal, we have described the use of direct finite-time Lyapunov exponents to study differential equation models of transient response networks. DLEs measure the separation between initially nearby trajectories in phase-space. We have used DLEs to identify sensitive regions of phase-space where small changes in the initial concentrations of network species alter cell fate (Figure 2). The separation can be calculated at any specific point in time, permitting prior biological knowledge concerning the most relevant experimental measurements to be leveraged. DLEs enable an exhaustive, multidimensional analysis of transient signals because they measure trajectory separation with respect to each dimension across the entire phase-space. As a result, DLEs are capable of identifying both important network interactions and in what context they affect signaling (*i.e.*, at what time or under which sets of initial conditions). By searching phase-space for sensitive initial conditions (those with large DLEs), we can identify surfaces (separatrices) that separate different classes of signals. A separatrix specifies critical combinations of species concentrations around which signaling

changes qualitatively. Because we can visualize the separatrix in different regions of phase-space, DLE analysis enables us to quantitatively interpret complex signaling interactions.

In applying DLE analysis to other biological signaling networks, a few considerations must be explored. DLE analysis is a numerical method which is flexible in the grid resolution and finite-times chosen for evaluation. While this flexibility is an asset for studying biological systems which have different time scales and varying parameter sensitivities, crude choices of time and phase-space grid may not capture all separatrices of interest. Because of the continuous dependence of trajectories on initial conditions, however, the DLE computation is a convergent procedure: refined grids and longer integration times are guaranteed to capture all separatrices. A second consideration is the relative strength of rates at which trajectories diverge at different locations in phase-space. Large rates of divergence will dominate the calculations, possibly obscuring smaller but biologically important trajectory separations. Therefore, it is important to select visualization methods that identify local features of the DLE field efficiently, thereby ensuring that all key behaviors are illuminated.

As a particular example of current biological interest, we applied DLE analysis to a model of caspase-3 activation involving caspase-8 and XIAP. The model responds to a pro-death stimulus with a transient signal leading to either death or survival. This network is an example of a transient response network: it has only one type of stable steady-state and the survival-vs-death decision is made before this steady-state is reached. This notion of transient response signaling in apoptosis differs from some previously published models, which have cast this phenomenon as a multiple steady-state problem and analyzed it accordingly [29, 30]. Although some insights concerning model parameter effects were gained in those contributions, recent experimental studies focused on dynamic and integrative measurement have demonstrated

that the key signals governing the phenotypic outcome of cell death-vs-survival are transient [28, 31]. Before stimulation, this network rests at a basal steady-state. Upon stimulation, a transient signal is produced during which the life-vs-death outcome is decided. Cells that survive return to the basal state. Thus, all key physiological signaling occurs during the transient phase.

While our model describes only a subset of the complex network regulating caspase-3, the model has eight species and is too complex to comprehensively characterize by inspection or parameter sensitivity analysis. Because DLE analysis is time-dependent and multivariate, we were able to gain specific insights about the regulation of caspase-3 that most likely would have been overlooked by inspection, single-parameter sensitivity analysis, or steady-state analysis (Figure 5F). Large DLEs defined a separatrix, from which we were able to gain quantitative, multivariate insight into the death-vs-survival decision. The separatrix classified two types of transient signals and defined the conditions leading to apoptosis and survival (Figure 4). We observed that the shape of the separatrix is not a simple plane and its shape and slope are dependent on rate constants. This suggests that in cases where reactions rates are hard to measure, the constant could be fit by comparing an experimentally identified separatrix with computationally predicted separatrices.

We envision DLE analysis as a tool for addressing challenging practical problems such as understanding the role of cell population heterogeneity in disease diagnosis and treatment. Others have described how population averages differ from the behavior of single cells by using population heterogeneity [18, 29]. DLE analysis can be used to investigate a key tangential question: How does population heterogeneity of protein expression correlate with different single-cell behaviors in a population of cells? To study the effects of noise and variability in protein expression within a population of cells, we can compare the concentration distributions

of key proteins with separatrices. Intersections between these distributions and separatrices should correlate with heterogeneous responses. For example, when cells are treated with a saturating concentration of TNF, a death-inducing ligand, only approximately 60% of a population of HT-29 cells die [28]. While not understood in quantitative terms, the TNF receptor is known to activate both pro-survival and pro-apoptotic pathways. The pre-Death Inducing Signaling Complex (pre-DISC) activates the nuclear factor-κB (NF-κB) pathway (a pro-survival pathway which upregulates XIAP) before activating caspase-8 and the mitochondrial pathway. Activation of the mitochondrial pathway causes the mitochondria to release Smac, a pro-apoptotic protein which inhibits XIAP. It is likely that within a cell population, basal protein expression variation can affect network behavior by changing the concentrations of key regulatory proteins such as XIAP. In the future, the phase-space locations of HT-29 cells could be determined experimentally by measuring the distribution of caspase-3, caspase-8, and XIAP expression levels. By evaluating their proximities to the separatrix, we could determine if the distribution of protein expression levels in a cell population can cause a heterogeneous response to TNF treatment. Eventually, we anticipate that DLE analysis can help us understand the transformation of a cell from a healthy to diseased state, and identify what changes in species concentrations are required to move the diseased cell across the separatrix to a healthier condition.

5 ACKNOWLEDGEMENTS

The authors thank Suzanne Gaudet, John Albeck, John Burke, Sampsa Hautaniemi, Robert Szalai, and Laura Sontag for stimulating and helpful discussions. This work was supported by the NIGMS Cell Decision Processes Center grant (P50-GM68762) to PKS and DAL, and a U.S. Department of Energy Computational Science Graduate Fellowship to BBA.

6 REFERENCES

1. Huang, C.Y. and J.E. Ferrell, Jr., *Ultrasensitivity in the mitogen-activated protein kinase cascade.* Proc Natl Acad Sci U S A, 1996. **93**(19): p. 10078-83.
2. Kholodenko, B.N., et al., *Quantification of short term signaling by the epidermal growth factor receptor.* J Biol Chem, 1999. **274**(42): p. 30169-81.
3. Bhalla, U.S. and R. Iyengar, *Functional modules in biological signalling networks.* Novartis Found Symp, 2001. **239**: p. 4-13; discussion 13-5, 45-51.
4. Schoeberl, B., et al., *Computational modeling of the dynamics of the MAP kinase cascade activated by surface and internalized EGF receptors.* Nat Biotechnol, 2002. **20**(4): p. 370-5.
5. Novak, B. and J.J. Tyson, *Modelling the controls of the eukaryotic cell cycle.* Biochem Soc Trans, 2003. **31**(Pt 6): p. 1526-9.
6. Bhalla, U.S., *Models of cell signaling pathways.* Curr Opin Genet Dev, 2004. **14**(4): p. 375-81.
7. Nelson, D.E., et al., *Oscillations in NF-{kappa}B Signaling Control the Dynamics of Gene Expression.* Science, 2004. **306**(5696): p. 704-708.
8. Davidson, E.H., et al., *A provisional regulatory gene network for specification of endomesoderm in the sea urchin embryo.* Dev Biol, 2002. **246**(1): p. 162-90.
9. Kitano, H., *Systems biology: a brief overview.* Science, 2002. **295**(5560): p. 1662-4.
10. Hornberg, J.J., et al., *Control of MAPK signalling: from complexity to what really matters.* Oncogene, 2005. **24**(36): p. 5533-42.
11. Thattai, M. and A. van Oudenaarden, *Attenuation of noise in ultrasensitive signaling cascades.* Biophys J, 2002. **82**(6): p. 2943-50.
12. Rosenfeld, N., et al., *Gene regulation at the single-cell level.* Science, 2005. **307**(5717): p. 1962-5.
13. Lidstrom, M.E. and D.R. Meldrum, *Life-on-a-chip.* Nat Rev Microbiol, 2003. **1**(2): p. 158-64.
14. Chong, H., H.G. Vikis, and K.L. Guan, *Mechanisms of regulating the Raf kinase family.* Cell Signal, 2003. **15**(5): p. 463-9.
15. Tyson, J.J., K.C. Chen, and B. Novak, *Sniffers, buzzers, toggles and blinkers: dynamics of regulatory and signaling pathways in the cell.* Curr Opin Cell Biol, 2003. **15**(2): p. 221-31.
16. Resat, H., et al., *An integrated model of epidermal growth factor receptor trafficking and signal transduction.* Biophys J, 2003. **85**(2): p. 730-43.
17. Hatakeyama, M., et al., *A computational model on the modulation of mitogen-activated protein kinase (MAPK) and Akt pathways in heregulin-induced ErbB signalling.* Biochem J, 2003. **373**(Pt 2): p. 451-63.
18. Hua, F., et al., *Effects of Bcl-2 levels on Fas signaling-induced caspase-3 activation: molecular genetic tests of computational model predictions.* J Immunol, 2005. **175**(2): p. 985-95.
19. Sasagawa, S., et al., *Prediction and validation of the distinct dynamics of transient and sustained ERK activation.* Nat Cell Biol, 2005. **7**(4): p. 365-73.

20. Bhalla, U.S., P.T. Ram, and R. Iyengar, *MAP kinase phosphatase as a locus of flexibility in a mitogen-activated protein kinase signaling network.* Science, 2002. **297**(5583): p. 1018-23.
21. Lauffenburger, D.A., *Cell signaling pathways as control modules: complexity for simplicity?* Proc Natl Acad Sci U S A, 2000. **97**(10): p. 5031-3.
22. Swameye, I., et al., *Identification of nucleocytoplasmic cycling as a remote sensor in cellular signaling by databased modeling.* Proc Natl Acad Sci U S A, 2003. **100**(3): p. 1028-33.
23. Bentele, M., et al., *Mathematical modeling reveals threshold mechanism in CD95-induced apoptosis.* J Cell Biol, 2004. **166**(6): p. 839-51.
24. Mendes, P. and D. Kell, *Non-linear optimization of biochemical pathways: applications to metabolic engineering and parameter estimation.* Bioinformatics, 1998. **14**(10): p. 869-83.
25. Markevich, N.I., J.B. Hoek, and B.N. Kholodenko, *Signaling switches and bistability arising from multisite phosphorylation in protein kinase cascades.* J Cell Biol, 2004. **164**(3): p. 353-9.
26. Tyson, J.J., A. Csikasz-Nagy, and B. Novak, *The dynamics of cell cycle regulation.* Bioessays, 2002. **24**(12): p. 1095-109.
27. Pomerening, J.R., S.Y. Kim, and J.E. Ferrell, Jr., *Systems-level dissection of the cell-cycle oscillator: bypassing positive feedback produces damped oscillations.* Cell, 2005. **122**(4): p. 565-78.
28. Gaudet, S., et al., *A compendium of signals and responses triggered by prodeath and prosurvival cytokines.* Mol Cell Proteomics, 2005. **4**(10): p. 1569-90.
29. Eissing, T., et al., *Bistability analyses of a caspase activation model for receptor-induced apoptosis.* J Biol Chem, 2004. **279**(35): p. 36892-7.
30. Bagci, E.Z., et al., *Bistability in Apoptosis: Roles of Bax, Bcl-2 and Mitochondrial Permeability Transition Pores.* Biophys J, 2005.
31. Janes, K.A., et al., *A systems model of signaling identifies a molecular basis set for cytokine-induced apoptosis.* Science, 2005. **310**(5754): p. 1646-53.
32. Hengartner, M.O., *The biochemistry of apoptosis.* Nature, 2000. **407**(6805): p. 770-6.
33. Danial, N.N. and S.J. Korsmeyer, *Cell death: critical control points.* Cell, 2004. **116**(2): p. 205-19.
34. Shi, Y., *Mechanisms of caspase activation and inhibition during apoptosis.* Mol Cell, 2002. **9**(3): p. 459-70.
35. Boatright, K.M., et al., *A unified model for apical caspase activation.* Mol Cell, 2003. **11**(2): p. 529-41.
36. Suzuki, Y., et al., *X-linked inhibitor of apoptosis protein (XIAP) inhibits caspase-3 and -7 in distinct modes.* J Biol Chem, 2001. **276**(29): p. 27058-63.
37. Salvesen, G.S. and C.S. Duckett, *IAP proteins: blocking the road to death's door.* Nat Rev Mol Cell Biol, 2002. **3**(6): p. 401-10.
38. Haller, G., *Distinguished material surfaces and coherent structures in three-dimensional fluid flows.* Physica D, 2001. **149**(4): p. 248-277.
39. Haller, G., *Lagrangian coherent structures from approximate velocity data.* Physics of Fluids, 2002. **14**(6): p. 1851-1861.
40. Wang, Y., et al., *Closed-loop Lagrangian separation control in a bluff body shear flow model.* Physics of Fluids, 2003. **15**(8): p. 2251-2266.

41. El Rifai, K., Bajaj, A. K., Haller, G., *Global dynamics of an autoparametric spring-mass-pendulum system and rigid body dynamics.* submitted to Nonlinear Dynamics, 2005.
42. Deveraux, Q.L., et al., *Cleavage of human inhibitor of apoptosis protein XIAP results in fragments with distinct specificities for caspases.* Embo J, 1999. **18**(19): p. 5242-51.

7 TABLES

parameter	value	units
k_1	2.67×10^{-9}	$cell*(s*molec)^{-1}$
k_{d1}	1×10^{-2}	s^{-1}
k_{d2}	8×10^{-3}	s^{-1}
k_3	6.8×10^{-8}	$cell*(s*molec)^{-1}$
k_{d3}	5×10^{-2}	s^{-1}
k_{d4}	1×10^{-3}	s^{-1}
k_5	7×10^{-5}	$cell*(s*molec)^{-1}$
k_{d5}	1.67×10^{-5}	s^{-1}
k_{d6}	1.67×10^{-4}	s^{-1}

Table 1. Parameter values, units, and sources.

Parameter names include the reaction number and "d" for dissociation constants. All parameters except for k_{d5} and k_{d6} were derived from a physico-chemical model fit to quantitative data from time courses of HT-29 human colon carcinoma cells treated with TNF [B. Schoeberl, S. Gaudet, D. Lauffenburger, and P. Sorger, unpublished results]. k_{d5} was derived using parameters in [42]. The ubiquitination rate, k_{d6}, was assumed to correlate with an average delay of 100 minutes between ubiquitination tagging and degradation.

8 FIGURE LEGENDS

Figure 1. Schematic of mathematical model for caspase-3 activation.

Caspase-3 (casp-3) activity is regulated by caspase-8 (casp-8) and XIAP. Caspase-8 (an initiator caspase) activates caspase-3 (an effector caspase) after forming a complex. Positive feedback is similarly accomplished through activation of caspase-8 by caspase-3. XIAP inhibits active caspase-3 by tagging it for ubiquitination and degradation. Here, a star indicates the active form of the caspases, a colon indicates a complex, and 'ub' indicates ubiquitination tagging. Labels in blue and green correspond with species and reaction numbers, respectively.

Figure 2. Large DLEs identify the location of maximum separation between trajectories, defining a separatrix.

Direct finite-time Lyapunov exponents (DLEs) measure local sensitivity to initial conditions. Relative to the time point used in the calculation of the exponent, small DLEs indicate little sensitivity (green). Large exponents indicate high sensitivity near the initial conditions (purple).

Figure 3. Time-course simulations show transient death and survival responses under two different initial conditions of XIAP.

(A) With little XIAP (2.9×10^3 molecules/cell) to inhibit activation of caspase-3, caspase-3 activation is sustained and destines this cell for death. In these time courses, the initial conditions were 0 molecules/cell for intermediate complexes and active caspase-3, 1×10^5 molecules/cell for active caspase-8, 1.34×10^5 molecules/cell for inactive caspase-8, and 2.67×10^5 molecules/cell for inactive caspase-3.

(B) With more XIAP (2.9 x10^4 molecules/cell), the pulse of caspase-3 activity is small and destines this cell for survival.

(C,D) A longer time course shows that both apoptotic and non-apoptotic signals arrive at the same type of fixed point. The simulation conditions are the same as in (A) and (B), respectively.

Figure 4. The six-hour DLE defines a separatrix separating phase-space into pro- and anti-apoptotic decisions.

Phase-space subplots are shown on a linear scale with initial conditions of XIAP and the active caspases ranging from 1 x 10^2 to 1 x 10^5, and 1 x 10^2 to 3.5 x 10^5 molecules/cell for the inactive caspases. All concentrations refer to initial conditions. The subspaces plotted were chosen to closely match the protein concentrations in untreated HT-29 cells [S. Gaudet and K. Leitermann, personal communication].

(A,B) Large DLEs of the caspase-3 activation network at six hours defines a separatrix. The blue curve is the separatrix which divides the phase-space into regions where cells survive (to the right of the separatrix) or die (to the left of the separatrix). (A) DLEs are shown in a subspace containing XIAP, active caspase-8, and inactive caspase-8 with 2.6 x 10^5 molecules/cell of inactive caspase-3 and 1 x 10^2 molecules/cell of active caspase-3 and the intermediate complexes. The gray curve highlights the separatrix, while the pro- and anti-apoptotic regions are outlined in red and green, respectively. (B) DLEs are shown in the subspace containing XIAP, active caspase-8, and active caspase-3 with 2.6 x 10^5 molecules/cell of inactive caspase-3 and inactive caspase-8, and 1 x 10^2 molecules/cell of the intermediate complexes. The stars indicate reference points (individual cells with different protein levels). The red and purple cells are pro-apoptotic while the green and orange cells are anti-apoptotic.

(C) The separatrix shape is sensitive to rate constants. As the rate of ubiquitination is decreased (k_{d6} increased), the slope of the separatrix increases. The DLEs are shown in the subspace containing XIAP and active caspase-8, with 2.6 x 10^5 molecules/cell of inactive caspase-3 and inactive caspase-8, and 1 x 10^2 molecules/cell of the intermediate complexes and active caspase-3. From low to high, the rate constant k_{d6} has values 3.33 x 10^{-5}, 1.67 x 10^{-4}, and 8.3 x 10^{-4} s^{-1}.

Figure 5. Stability and steady-state analyses of the caspase-3 activation network model.
(A) Stability analysis shows one stable (purple) and three unstable (green) types of fixed points (Supplementary Materials). Every type of fixed point requires concentrations of zero for the intermediate complexes. For each of the four fixed point types, there are two or three species that can be nonzero. The green (unstable) and purple (stable) circles indicate which species can be nonzero for each type of fixed point.
(B-E) The steady-state locations in the caspase-3 activation network are not globally clustered. The fixed points are plotted in the subspace containing active and inactive caspase-8, with increasing initial concentrations of inactive caspase-8: (B) 8.8 x 10^4, (C) 18 x 10^5, and (D) 3.5 x 10^5 molecules/cell. Other initial conditions were 2.6 x 10^5 molecules/cell of inactive caspase-3, 1 x 10^2 molecules/cell of active caspase-3 and the intermediate complexes, and 1 x 10^2 – 1 x 10^5 molecules/cell for active caspase-8 and XIAP. For each initial concentration of inactive caspase-8 (B-D), the steady-states are moderately clustered and are segregated by large DLEs (blue). However, the fixed points from different inactive caspase-8 initial conditions do not cluster when plotted together (E).
(F) A schematic compares the use of steady-state and DLE analysis methods. In systems where steady-states localize to different regions of phase-space (left), steady-state analysis methods

may be used to characterize the phenotypic behavior of the network. DLE analysis can distinguish between behaviors in networks regardless of fixed point clustering.

Figure 1

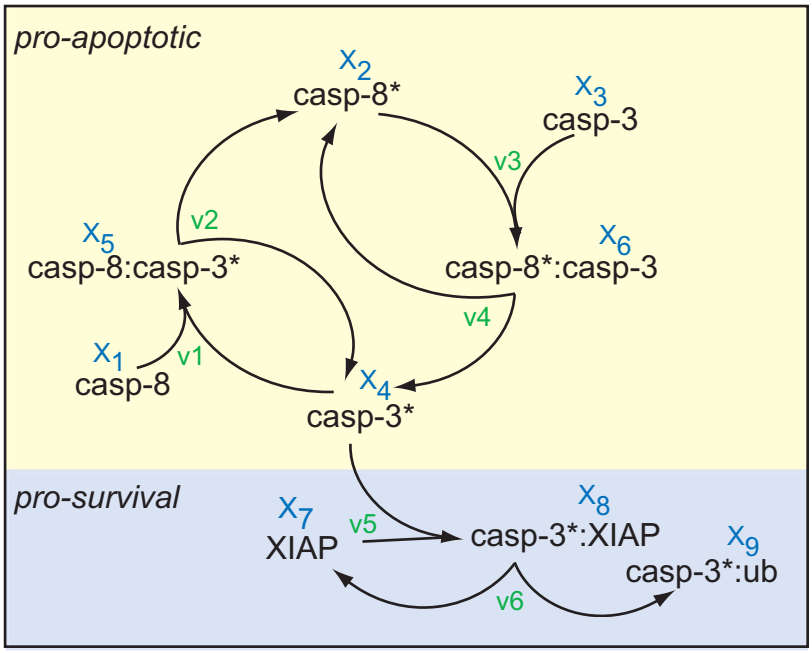
pro-apoptotic
X2
casp-8*
X3
casp-3
v3
v2
X5
casp-8:casp-3*
X6
casp-8*:casp-3
v4
X1
casp-8
v1
X4
casp-3*
pro-survival
X7
XIAP
v5
X8
casp-3*:XIAP
X9
casp-3*:ub
v6

Figure 2

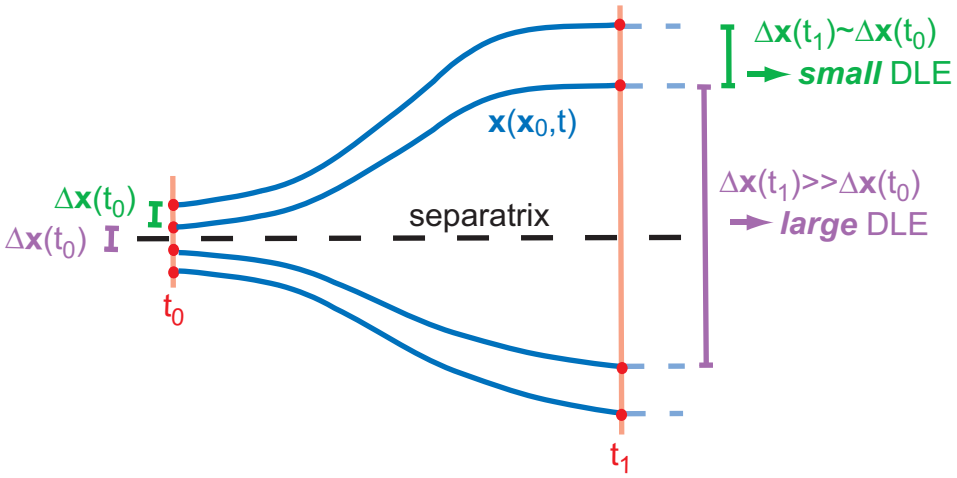
Δx(t1)~Δx(t0)
small DLE
x(x0,t)
Δx(t1)>>Δx(t0)
large DLE
Δx(t0)
Δx(t0)
separatrix
t0
t1

Figure 3

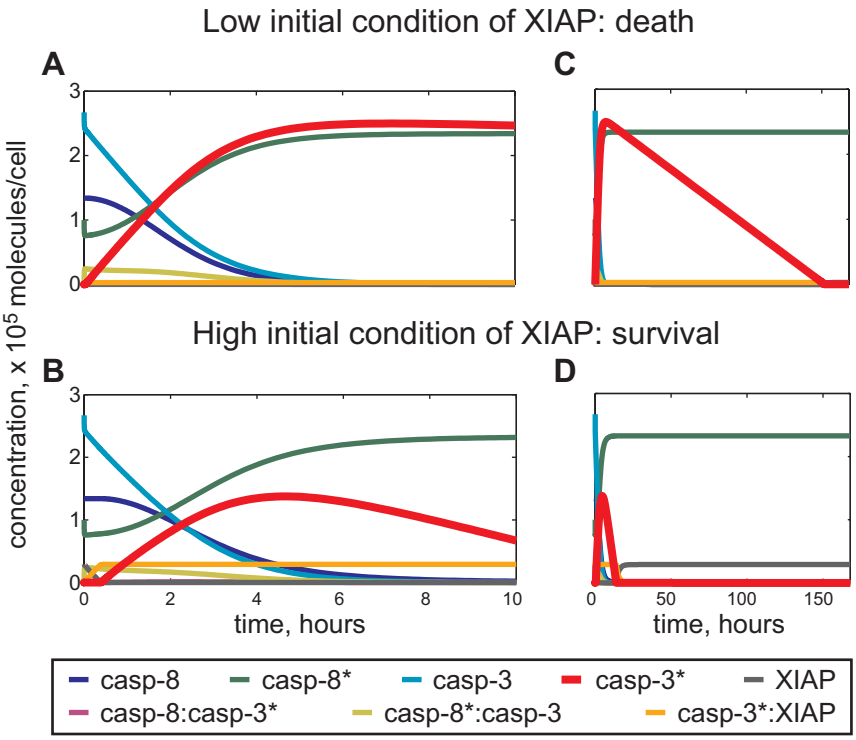
Low initial condition of XIAP: death
A
C
High initial condition of XIAP: survival
B
D
concentration, x 10^5 molecules/cell
time, hours
time, hours
casp-8
casp-8*
casp-3
casp-3*
XIAP
casp-8:casp-3*
casp-8*:casp-3
casp-3*:XIAP

Figure 4

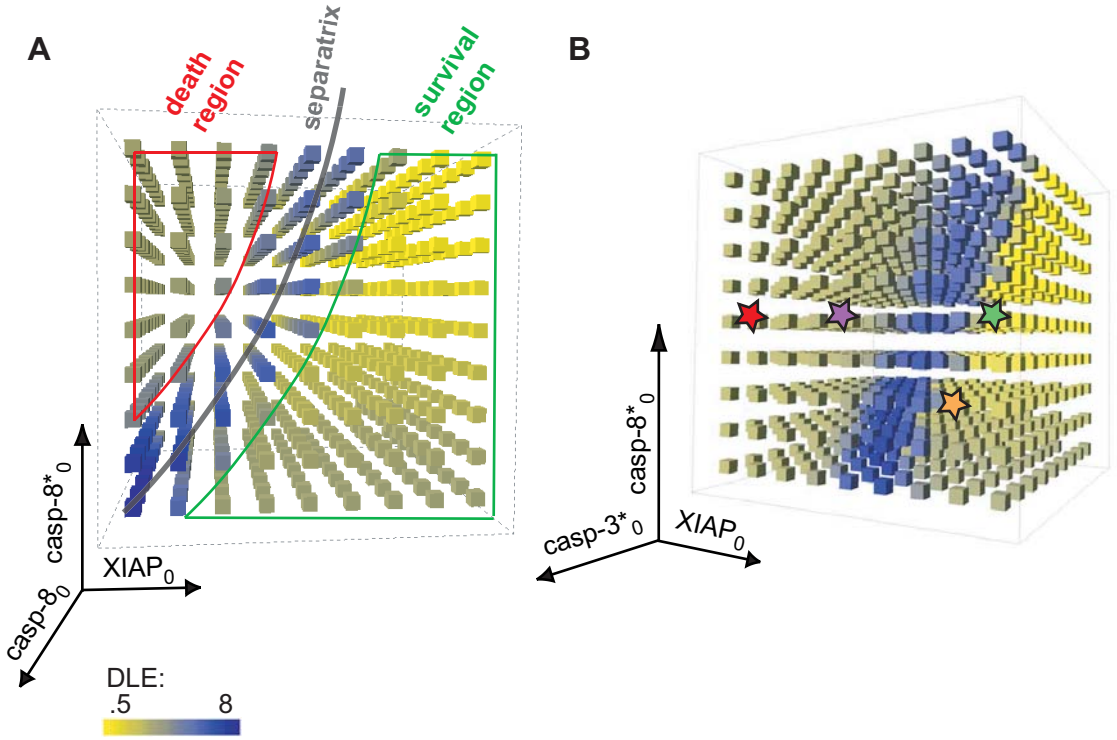
A
death region
separatrix
survival region
casp-8*0
XIAP0
casp-80
DLE:
.5
8
B
casp-8*0
casp-3*0
XIAP0
C
Low kd6
Medium kd6
High kd6
casp-8*0
XIAP0

Figure 5

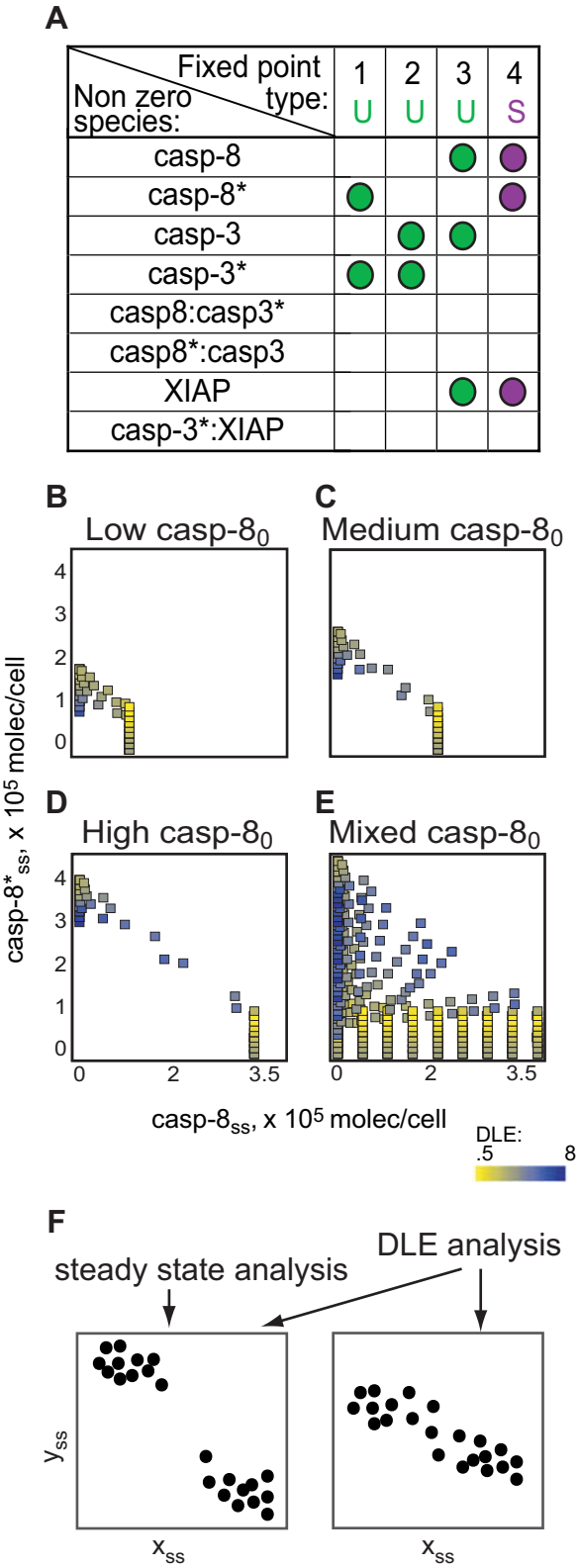
A
Fixed point
Non zero species:
type:
1 U
2 U
3 U
4 S
casp-8
casp-8*
casp-3
casp-3*
casp8:casp3*
casp8*:casp3
XIAP
casp-3*:XIAP
B
Low casp-8$_0$
C
Medium casp-8$_0$
D
High casp-8$_0$
E
Mixed casp-8$_0$
casp-8*$_{ss}$, x 10^5 molec/cell
casp-8$_{ss}$, x 10^5 molec/cell
DLE:
.5
8
F
steady state analysis
DLE analysis
y_{ss}
x_{ss}
x_{ss}

9 SUPPLEMENTARY MATERIALS

9.1 Fixed point criterion

To solve for the fixed points, we note that the listed rate parameters are nonzero. By definition of a fixed point, we set derivates of each species to zero:

$$0 = -k_1 x_4 x_1 + k_{d1} x_5 \quad (17)$$
$$0 = k_{d2} x_5 - k_3 x_2 x_3 + k_{d3} x_6 + k_{d4} x_6 \quad (18)$$
$$0 = -k_3 x_2 x_3 + k_{d3} x_6 \quad (19)$$
$$0 = k_{d4} x_6 - k_1 x_4 x_1 + k_{d1} x_5 - k_5 x_7 x_4 + k_{d5} x_8 + k_{d2} x_5 \quad (20)$$
$$0 = -k_{d2} x_5 + k_1 x_4 x_1 - k_{d1} x_5 \quad (21)$$
$$0 = -k_{d4} x_6 + k_3 x_2 x_3 - k_{d3} x_6 \quad (22)$$
$$0 = -k_5 x_7 x_4 + k_{d5} x_8 + k_{d6} x_8 \quad (23)$$
$$0 = k_5 x_7 x_4 - k_{d5} x_8 - k_{d6} x_8 \quad (24)$$

Substituting (17) into (21):

$$k_{d2} x_5 = 0 \Rightarrow x_5 = 0. \quad (25)$$

Substituting (19) and (25) into (18):

$$k_{d4} x_6 = 0 \Rightarrow x_6 = 0. \quad (26)$$

Substituting (25) into (17):

$$x_4 x_1 = 0. \quad (27)$$

Substituting (25), (26), and (27) into (20):

$$k_5 x_7 x_4 = k_{d5} x_8 \quad (28)$$

Rewriting (24):

$$k_5 x_7 x_4 = (k_{d5} + k_{d6}) x_8. \quad (29)$$

Comparing (28) and (29),

$$(k_{d5} + k_{d6}) x_8 = k_{d5} x_8 \ . \quad (30)$$

Because we have assumed that the rate constants are nonzero,

$$x_8 = 0 \quad (31)$$

Substituting (15) into (12)

$$x_7 x_4 = 0 \quad (32)$$

From equations (9), (10), (11), (15), and (16) we can derive steady-state conditions:

$$x_5 = x_6 = x_8 = 0 \quad (33)$$
$$x_4 OR(x_1 AND x_7) = 0, \quad (34)$$
$$x_2 OR x_3 = 0 \quad (35)$$

Together, these define conditions for the four types of fixed points in the system (Figure 5A).

9.2 Determination of stability

The stability of each type of fixed point (listed in Figure 5A) was deduced using conservation relations and type-specific steady state conditions (equations 33-35). This is convenient since traditional stability analysis would have been extremely difficult for this 8-dimensional system. At each fixed point, there are 2-4 zero eigenvalues, making stability analysis methods based on linearization inconclusive. The number of zero eigenvalues was determined symbolically using Maple 9 (Waterloo Maple Inc., Ontario, Canada).

- Fixed point type 1: All species must have zero concentrations except active caspse-8 and active caspase-3. Since XIAP concentration is zero (there is no turnover of XIAP in the model and XIAP is not initially present), active caspase-3 cannot form complexes with XIAP. Therefore, the concentration of caspase-3 and caspase-8 will not change. These fixed points are unstable because perturbations of XIAP concentrations to nonzero values send these trajectories to fixed point type 4.

Biologically, these fixed points would represent cells signaling for death because all of the caspases are active. These fixed points are attracting in some directions because the pulse peaks approach these fixed points before declining towards fixed point type 4 (Figure 3). In comparing trajectories from above and below the separatrix, we noticed that the peak of caspase-3 activation corresponds to this type of unstable fixed point. The height of the pulse corresponds with its width. For example, in Figure 3C, the active caspase-3 pulse is tall and wide while in Figure 3D, the pulse is short and narrow. The unstable fixed point is attracting in some directions; therefore, the closer the trajectory moves towards this unstable fixed point, the stronger the pro-apoptotic pull. This attraction to the unstable fixed point is what resulted in higher and wider active caspase-3 pulses.

We therefore defined a pulse metric to explore the relationship between the pulse and the network outcome. Since we hypothesized that the pulse magnitude and width corresponded with its proximity to these unstable fixed points, we defined a pulse metric as the shortest distance between the trajectory and fixed point 1. For the time courses shown in Figures 3A-B, the pulse metrics are 1.3×10^4 and 1.4×10^5 for low and high initial conditions of XIAP, respectively. In Figure S1, the pulse metric is plotted in the same phase-space slice displayed for the DLEs in Figure 4A. This metric divides the phase space similar to the separatrix defined by high DLEs. Above the separatrix, the pulse metric is small, indicating that those trajectories are strongly attracted to these fixed points. In being so strongly pulled away from the steady state by this unstable fixed point, these systems have made a death decision. For the initial conditions where the pulse metric is large (under the separatrix), the trajectories are far enough away from the unstable fixed point to avoid being pulled away from the steady state. As a result, caspase-3 is not strongly activated and these systems avoid apoptosis.

- Fixed point type 2: All species must have zero concentrations except caspase-3 and active caspase-3. Since there is no synthesis of caspase-8 and XIAP in this model any species containing a form of caspase-8 or XIAP (including all intermediates complexes) will be absent. These fixed points are unstable because perturbations of caspase-8 and XIAP concentrations to nonzero values send these trajectories to fixed point type 4. This type of fixed point would represent an extremely rare (or knock-out) cell with no caspase-8 or XIAP.

- Fixed point type 3: All species have zero concentrations except caspase-3, caspase-8, and XIAP. Since there are no active caspases, intermediate complexes cannot be formed. These fixed points are unstable because perturbations in the active caspases or intermediate complexes to nonzero values send these trajectories to fixed point type 4. Biologically, this type of fixed point represents a cell that has not received a death signal.

- Fixed point type 4: All species have zero concentrations except caspase-8, active caspase-8, and XIAP. This fixed point is the most general, and almost all biologically significant initial conditions will fall under this scenario: caspase-8 is converted into active caspase-8 while caspase-3 is converted into active caspase-3 until XIAP causes all of the active caspase-3 to be degraded. Given ample time, all of the caspase-3 in the system is degraded and nonzero concentrations for caspase-8, active caspase-8, and XIAP may remain. This type of fixed point is stable because under perturbations to the caspases, intermediate complexes, or XIAP, the network will return to this type of fixed point. Biologically, this type is fixed point would

represent the state of the network after it is responded (with a transient behavior) to a death-signal before the system is reset (not modeled here).

9.3 Caspase-3 activation model with protein turnover

Our model was simplified to by omitting protein synthesis and degradation. A similar analysis was performed with a model extended to include turnover and cleavage of XIAP by active caspase-3. This extended model yielded similar results to the simplified model (Figures S2 and S3). A constitutive degradation rate, k_{deg}, was assumed for all species; it was estimated as 4.63 x 10^{-5} (s^{-1}) using the half-life of pro-caspase-3 [S1]. The synthesis rate was assumed to be the product of k_{deg} and the initial concentration of the protein for pro-caspase-3, pro-caspase-9, and XIAP. The model is specified below (equations 36-43). The rate of XIAP cleavage by active caspase-3, k_{clv}, is 5 x 10^{-6} (s^{-1}) [S2]. Species numbers and non-turnover parameters are identical to the basic model described in Figure 1 and Table 1.

$$\dot{x}_1 = -k_1 x_4 x_1 + k_{d1} x_5 - k_{\text{deg}} x_1 + k_{\text{deg}} x_1(t=0) \quad (36)$$

$$\dot{x}_2 = k_{d2} x_5 - k_3 x_2 x_3 + k_{d3} x_6 + k_{d4} x_6 - k_{\text{deg}} x_2 \quad (37)$$

$$\dot{x}_3 = -k_3 x_2 x_3 + k_{d3} x_6 - k_{\text{deg}} * x_3 + k_{\text{deg}} x_3(t=0) \quad (38)$$

$$\dot{x}_4 = k_{d4} x_6 - k_1 x_4 x_1 + k_{d1} x_5 - k_5 x_7 x_4 + k_{d5} x_8 + k_{d2} x_5 - k_{\text{deg}} x_4 \quad (39)$$

$$\dot{x}_5 = -k_{d2} x_5 + k_1 x_4 x_1 - k_{d1} x_5 - k_{\text{deg}} x_5 \quad (40)$$

$$\dot{x}_6 = -k_{d4} x_6 + k_3 x_2 x_3 - k_{d3} x_6 - k_{\text{deg}} x_6 \quad (41)$$

$$\dot{x}_7 = -k_5 x_7 x_4 + k_{d5} x_8 + k_{d6} x_8 - k_{\text{deg}} x_7 - k_{clv} x_7 x_4 + k_{\text{deg}} x_7(t=0) \quad (42)$$

$$\dot{x}_8 = k_5 x_7 x_4 - k_{d5} x_8 - k_{d6} x_8 - k_{\text{deg}} x_8 \quad (43)$$

.

10 SUPPLEMENTARY FIGURE LEGENDS

Figure S1. A distance metric defines a separatrix.

A phase-space subplot of the distance metric (shortest distance to type 1 fixed points) is shown on a linear scale under the conditions shown for the DLE-defined separatrix in Figure 4A The separatrix matching the DLE-defined separatrix is between small (blue) and large (red) distances. The distance is large below the separatrix (survival) and small above the separatrix (death).

Figure S2. Time-course simulations show transient death and survival responses under two different initial conditions of XIAP when turnover is introduced to the model.

In these time courses, the initial conditions matched those in Figure 3A-B, respectively. Under a low initial concentration of XIAP (A), the transient caspase-3 pulse is taller and wider than the pulse under a higher initial concentration of XIAP.

Figure S3. The six-hour DLE defines a separatrix separating phase-space into pro- and anti-apoptotic decisions in a model including turnover.

The six-hour DLEs are plotted under the conditions in Figure 4A. The introduction of protein turnover to the caspase-3 activation model did not significantly change the shape or the location of the separatrix.

11 SUPPLEMENTARY REFERENCES

S1. DiPietrantonio, A.M., et al., *Fenretinide-induced caspase 3 activity involves increased protein stability in a mechanism distinct from reactive oxygen species elevation.* Cancer Res, 2000. **60**(16): p. 4331-5.

S2. Eissing, T., et al., *Bistability analyses of a caspase activation model for receptor-induced apoptosis.* J Biol Chem, 2004. **279**(35): p. 36892-7.

Figure S1

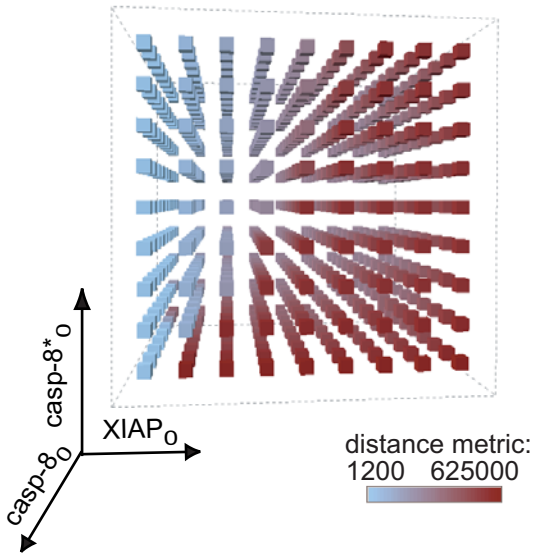

Figure S2

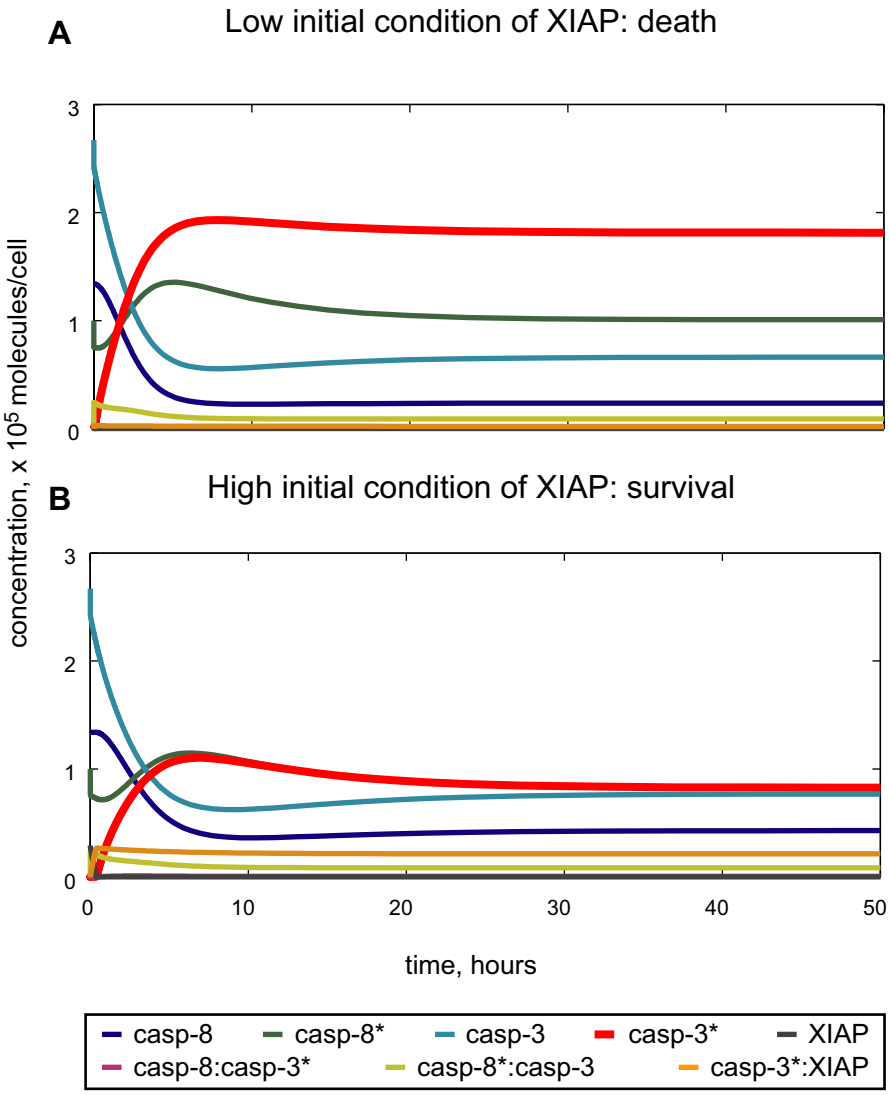
A
Low initial condition of XIAP: death
B
High initial condition of XIAP: survival
concentration, x 10^5 molecules/cell
time, hours
0
1
2
3
0
10
20
30
40
50
casp-8
casp-8*
casp-3
casp-3*
XIAP
casp-8:casp-3*
casp-8*:casp-3
casp-3*:XIAP

Figure S3